ABORT TRAJECTORY DESIGN STRATEGIES FOR THE ARTEMIS MISSIONS

Brian McCarthy, Josh Geiser, Matt Bolliger, Daniel Owen, and Damennick Henry

NASA's Artemis campaign plans to send astronauts to the lunar surface for the first time since 1972. The campaign relies on the Orion crew capsule to ferry the crew from Earth to an L_2 9:2 lunar synodic resonant Near-Rectlinear Halo Orbit (NRHO) before descent to the lunar surface. This investigation examines a process to construct various abort families during transit from Earth to the NRHO using the Earth-Moon Circular Restricted Three-Body Problem (CR3BP). The initial trajectories are constructed using the CR3BP and categorized in families. A process is then summarized to transcribe and converge trajectories from the CR3BP into a higher-fidelity model. Ultimately, an effective methodology to develop, classify and converge these aborts in higher-fidelity is critical to the Artemis program in the event of an anomaly during the crew transit.

INTRODUCTION

In November 2022, the Artemis I mission launched to test the Orion crew capsule, representing the first component of the campaign to develop a sustaining human presence in cislunar space. Artemis II, the first crewed mission of the Orion vehicle, is planned for November 2025; it will fly a free-return trajectory around the Moon. Subsequently, the first crewed landing on the lunar surface since 1972 is planned on Artemis III, leveraging an Earth-Moon L2 Near-Rectilinear Halo Orbit (NRHO) as the staging location for Orion and the Human Landing System (HLS) before descent to the lunar surface.² The Artemis IV+ missions plan to include the lunar Gateway station within the concept of operations en route to the lunar surface. Each of these missions is increasingly complex and demands extensive trajectory analysis to ensure accomplishment of all the mission objectives. One aspect of the trajectory design problem for the Artemis campaign is understanding and constructing aborts along each of the nominal missions in the event of an anomaly. Many abort trajectory options are constructed, optimized, and analyzed prior to launch to provide an understanding of the times-of-flight and propellant costs to return to Earth. In this investigation, methodologies are examined to construct abort trajectories along various phases of the mission, transcribe them into an optimization process, and ultimately optimize in a higher-fidelity model. To construct initial families of trajectories, the Earth-Moon Circular Restricted Three-Body Problem (CR3BP) is leveraged to characterize the fundamental motion of the abort trajectory options and provide an initial guess to a higher-fidelity dynamics model. Methods of constructing initial abort trajectory geometries are discussed using periapsis Poincaré maps. A multi-parameter continuation algorithm is discussed to construct families of Δv optimal abort trajectory solutions in the CR3BP. Examples of various abort geometries are discussed for various phases along an Artemis III+ mission profile, with a focus on the more dynamically sensitive regions. Lastly, a transcription process is discussed that uses information from the CR3BP initial guesses to perform optimization in a higher-fidelity model. Development of various initial guesses and a methodology to transition the initial guesses is critical to analyzing all of the abort trajectory options for the Artemis campaign. A streamlined process ultimately

^{*}Artemis Mission Design Engineer, a.i. solutions, Inc., 2101 E NASA Pkwy, Houston, TX 77058; brian.p.mccarthy@nasa.gov

[†]Artemis Mission Design Engineer, NASA JSC, 2101 E NASA Pkwy, Houston, TX 77058; joshua.k.geiser@nasa.gov

[‡]Astrodynamics Engineer, Advanced Space, 1400 W 122nd Ave Suite 200, Westminster, CO

[§] Astrodynamics Engineer, Advanced Space, 1400 W 122nd Ave Suite 200, Westminster, CO

[¶]Postdoctoral Researcher, University of Colorado Boulder, 3775 Discovery Dr, Boulder, CO

provides decision makers more options and shorter processing time to execute in the event of an anomaly requiring an abort.

Several previous investigations have studied the lunar abort problem. During the Apollo program, several techniques were examined, depending on the phase of the mission.³ The performance of two-impulse returns were analyzed during translunar coast using the Apollo service propulsion system (SPS).⁴ Single and multi-impulse aborts were also investigated for non-free return trajectories.⁵ More recently, for the Constellation program, Condon et al. investigated translunar abort capabilities for various lunar mission configurations.⁶ Condon et al. also examined the abort capabilities in relation to various lunar landing sites.⁷ Earth-return trajectory planning techniques were investigated by Whitley et al. as well as Williams et al. using a patched conic approach.^{8,9} Robinson and Geller developed an Earth-return targeting algorithm using various conic approximations.¹⁰ Dong et al. summarized a method to construct lunar abort trajectories using an approach based on pseudostate theory.¹¹ During the Artemis I mission, abort planning was developed for all phases along the mission to test the Orion capsule in a distant retrograde orbit (DRO).^{12,13} To augment these previous methods, the current investigation employs techniques in the CR3BP to facilitate the generation of abort trajectories for various locations along an Artemis reference mission.

ARTEMIS III+ MISSION PROFILE

The crewed missions after Artemis II plan to operate in a 9:2 lunar synodic resonant NRHO before and after the lunar surface sorties. This orbit offers advantageous eclipse avoidance properties, low stationkeeping costs, extended visibility of the lunar south pole, constant line of sight with Earth and access to the lunar surface. The transit trajectory to arrive along the 9:2 NRHO requires three major maneuvers: a translunar injection maneuver (TLI) to depart Earth, an outbound powered flyby (OPF) at the lunar flyby, and the NRHO insertion maneuver (NRI) that allows Orion to insert into the NRHO. Two representative reference trajectory are rendered in Figure 1, with different outbound transit times-of-flight. Depending on the mission and the launch date, the time-of-flight from TLI to NRI varies between 5 and 11 days. Understanding the abort capabilities along various reference trajectories is critical to assessing the risk for all of the crewed Artemis missions beyond Artemis II, since each mission plans to use a similar transit trajectory. This investigation focuses on constructing various abort trajectory families for dynamically sensitive regions of the transit, where the gravitation forces of the Earth and Moon must both be considered. Specifically, the region of the transit after the TLI maneuver and before arrival into the NRHO. There are two main drivers when considering aborts during any of the Artemis III+ missions: propellant required to execute the abort to return safely to Earth and the amount of consumables the crew has for the duration of the mission. The amount of propellant, or Δv , available for an abort changes during the mission, depending on which maneuvers have been executed. As major maneuvers are executed along the reference trajectory for a nominal mission, there is less propellant available to execute an abort. The crew consumables drive the time-of-flight requirements for aborts as well. For example, if an anomaly occurs that requires an abort to Earth, it is assumed that the crew has approximately 21 days of consumables within the Orion capsule starting from launch. However, if a depressurization of the capsule occurs, the amount of crew consumables is reduced. Similarly, if the propulsion system is affected by the anomaly that requires the abort, the duration of the burns and/or the amount of propellant available may be reduced. All of these factors must be considered when selecting an abort option should one be required; therefore, an extensive understanding of the full abort trajectory solution space is critical in the event of an anomaly.

DYNAMICAL MODELS

Two dynamical models are leveraged in this investigation, the Circular Restricted Three-Body Problem (CR3BP) and a Sun-Earth-Moon ephemeris model. The CR3BP offers higher fidelity and additional behaviors in comparison to the two-body model. In this model, two gravitational bodies, denoted P_1 and P_2 , remain in circular Keplerian orbits about their mutual barycenter (i.e., center of mass). A third body, P_3 , moves under the gravitational influence of the two larger bodies and is assumed to be massless. The model is defined relative to a rotating coordinate system, where the $+\hat{x}$ direction is defined from the barycenter toward P_2 . The $+\hat{z}$ direction is defined parallel to the direction of the orbital angular momentum vector for

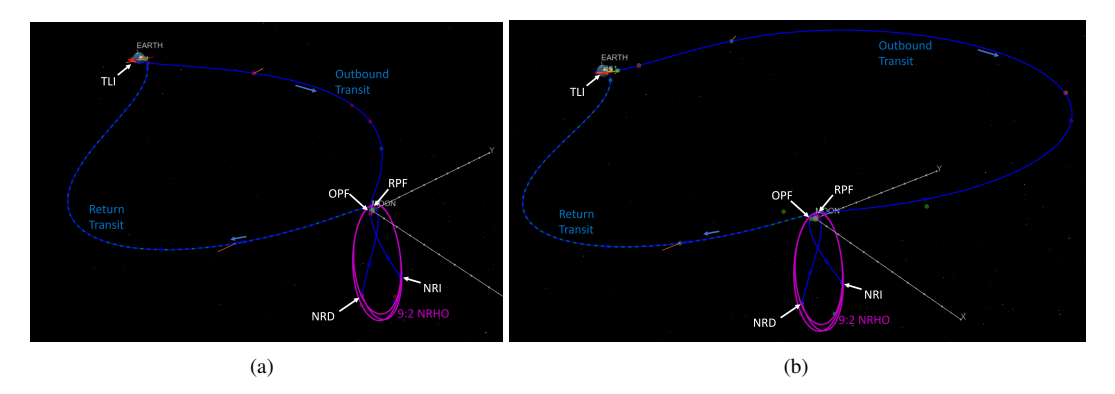


Figure 1. Representative Artemis III+ reference trajectories with (a) short outbound duration and (b) long outbound duration, rendered in the Earth-Moon rotating pulsating frame.

 P_1 and P_2 ; the \hat{y} direction completes the orthonormal triad. The position and velocity of P_3 relative to the barycenter in the rotating frame are defined as $\vec{x} = \begin{bmatrix} x & y & z & \dot{x} & \dot{y} & \dot{z} \end{bmatrix}^T$, where the first three and the last three elements are the position and relative velocity components, respectively. The equations of motion for a particle moving in the CR3BP are a set of three, second-order scalar differential equations of motion,

$$\ddot{x} - 2\dot{y} = \frac{\partial U^*}{\partial x} \qquad \qquad \ddot{y} + 2\dot{x} = \frac{\partial U^*}{\partial y} \qquad \qquad \ddot{z} = \frac{\partial U^*}{\partial z}$$
 (1)

The pseudo-potential is a scalar defined solely as a function of position and the CR3BP mass parameter, $\mu = M_2/(M_1 + M_2)$, where M_1 and M_2 are the masses of P_1 and P_2 , respectively.¹⁴ The pseudo-potential function takes the following form,

$$U^* = \frac{x^2 + y^2}{2} + \frac{\mu}{r} + \frac{1 - \mu}{d} \tag{2}$$

where $d=\sqrt{(x+\mu)^2+y^2+z^2}$ and $r=\sqrt{(x-1+\mu)^2+y^2+z^2}$ represent the distances of P_3 relative to P_1 and P_2 , respectively. The CR3BP admits a single integral of the motion, commonly denoted the Jacobi Constant (JC). The Jacobi Constant is a function of the pseudo-potential and the relative velocity magnitude expressed in the rotating reference frame,

$$JC = 2U^* - v^2 \tag{3}$$

where $v = \sqrt{\dot{x}^2 + \dot{y}^2 + \dot{z}^2}$. The Jacobi Constant is an energy-like quantity that characterizes motion in a CR3BP system and remains constant for all time over any ballistic arc propagated in the CR3BP. One advantage of the CR3BP model is that the system is time invariant, which is important for developing families of aborts that are agnostic to launch epoch. The CR3BP is also a good approximation for a multi-body environment and the trajectory characteristics generally persist when transitioning results to a higher-fidelity ephemeris model.

The ephemeris force model offers a higher-fidelity gravity force representation on the spacecraft by incorporating the ephemeris states of various celestial bodies. The interpolated position and velocity state corresponding to these bodies are extracted from the ephemerides on the JPL NAIF server.¹⁵ The analysis performed in the ephemeris model reinforces the result found in the CR3BP and represents a more realistic cislunar environment to execute a scenario during an Artemis mission.

OPTIMIZATION METHODS AND CONTINUATION

In this investigation, families of solutions are assessed in the CR3BP to understand the fundamental motion associated with cislunar abort trajectories and how to classify different families dynamically. Subsequently,

an optimization algorithm is paired with a multi-parameter continuation scheme to construct these families of solutions. The optimization method is summarized by Kaufman as well as Goodman, but is included for completeness to describe how it is paired with a multi-parameter continuation scheme developed by Henderson. $^{16-18}$ Consider a free-variable/constraint formulation of a differential corrections problem, where \bar{X} is defined as the free-variable vector and \bar{F} is the constraint vector

$$\bar{X} = \begin{bmatrix} x_1 & x_2 & \dots & x_n \end{bmatrix}^T \tag{4}$$

$$\bar{F} = \begin{bmatrix} F_1 & F_2 & \dots & F_m \end{bmatrix}^T = \bar{0} \tag{5}$$

where x_i is the i^{th} free-variable of n total free-variables, and F_j is the j^{th} scalar constraint of m total scalar equality constraints. It is also assumed that m < n, such that there are more free-variables than constraints. Next, consider a cost function, f, that is a function of the free-variables. An additional set of constraints are formulated to minimize or maximize f, defined,

$$\bar{F}_{\text{opt}} = \bar{\nabla} f \cdot \text{null}(D\bar{F})^T = \bar{0} \tag{6}$$

where $\bar{\nabla} f$ is the gradient of the cost function and $\operatorname{null}(D\bar{F})$ is an $n \times n - m$ matrix representing the nullspace basis of the Jacobian matrix of the differential corrections problem defined in Equation (4). The derivative of the optimality constraints with respect to the free-variables is defined,

$$\frac{D\bar{F}_{\text{opt}}}{D\bar{X}} = \bar{\nabla}^2 f \cdot \text{null}(D\bar{F}) + \bar{\nabla} f \cdot \frac{D(\text{null}(D\bar{F}))}{D\bar{X}}$$
 (7)

where $\bar{\nabla}^2 f$ is the Hessian of the cost function and the term $\frac{D(\text{null}(D\bar{F}))}{D\bar{X}}$ is summarized by Goodman using a QR decompisition to compute the nullspace basis of the Jacobian matrix. Alternatively, automatic differentiation can be leveraged to compute the derivative for ease of implementation. In this investigation, a singular value decomposition coupled with automatic differentiation is used to compute the nullspace basis and associated derivatives. By utilizing this optimization technique, the need to provide an initial guess for the Lagrange multipliers and to solve their associated costate equations during each iteration of the corrections process is removed in contrast to a typical SQP method.

The differential corrections process summarizes a method to solve for a single solution; however, in this investigation, families of solutions are of interest to classify various abort types. Trajectories within each family are characterized by two parameters, the total time-of-flight from the first abort maneuver to the entry interface state, i.e., the end of the in-space abort trajectory near Earth, defined $t_{\rm abort}$, and the time along the reference trajectory that the first abort maneuver is executed, defined $t_{\rm ref}$. These two variables are appended to the free-variable vector in Equation (4) such that there are n+2 free-variables. The resulting boundary value problem is defined,

$$\bar{X}_{\text{fam}} = \begin{bmatrix} x_1 & x_2 & \dots & x_n & t_{\text{ref}} & t_{\text{abort}} \end{bmatrix}^T$$
 (8)

$$\bar{F}_{fam} = \begin{bmatrix} F_1 & F_2 & \dots & F_m & \bar{F}_{opt} \end{bmatrix}^T \tag{9}$$

where \bar{F}_{fam} is a vector of length n and \bar{X}_{fam} is of length n+2. The optimization constraints are computed using the first n free-variables and do not include t_{ref} and t_{abort} because a locally optimal solution is desired for a given t_{ref} and t_{abort} in a family of solutions. The targeting problem defined in Equations (8) and (9) now has two degrees of freedom where a two-parameter family of solutions exists in the vicinity. To compute the family of solutions, a multi-parameter continuation method is used that extends pseudo-arclength continuation to problems with a tangent space greater than 1-dimension. This extends a similar scheme applied to NRHO rephasing to a problem with a higher-dimensional tangent space.¹⁹

Similar to pseudo-arclength continuation, the multi-parameter continuation scheme maps a family of solutions by leveraging the tangent space (i.e. the null space of $D\bar{F}_{\text{fam}}$) around previously computed solutions to calculate new solutions. More specifically, the procedure also successively computes orthogonal projections of vectors within a known solution's tangent space to continue along the family. The families considered in this

work are two-dimensional and therefore have two-dimensional tangent spaces. Given that $N_{\text{fam}} \in \mathbb{R}^{n+2\times 2}$ is a matrix with an orthonormal basis of the tangent space around a previously computed point \bar{X}_{fam}^* as its columns, the orthogonal projection must satisfy

$$\bar{F}_{con} = N_{fam}^{T} (\bar{X}_{fam} - \bar{X}_{fam}^{*} - N_{fam}\bar{s}) = \bar{0}$$
(10)

where $\bar{s} \in \mathbb{R}^2$ is a vector determining both the size and direction of the continuation step. Note that \bar{F}_{con} yields two more constraints that can be solved simulataneously with \bar{F}_{fam} to yield an $n+2 \times n+2$ system of equations. Effectively, \bar{F}_{con} is simply a higher-dimensional analog to the pseudo-arclength continuation constraint. Thus, the constraint in Equation (10) is appended to the constraint vector in Equation (9),

$$\bar{F}_{\text{mpc}} = \begin{bmatrix} F_1 & F_2 & \dots & F_m & \bar{F}_{\text{opt}} & \bar{F}_{\text{con}} \end{bmatrix}^T$$
 (11)

where now the dimension of $\bar{X}_{\rm fam}$ and $\bar{F}_{\rm mpc}$ are equal and the solution is solved using Newton's method.

The key additional complexity associated with multi-parameter continuation is the determination of the continuation direction (i.e. the direction of \bar{s}). Unlike pseudo-arclength continuation which continues along a curve of solutions in a single direction, the two-parameter continuation scheme must continue in multiple directions to compute a surface of solutions. To determine the continuation direction, the polygon update procedure developed by Henderson is leveraged. In the algorithm, polygons are defined within the tangent spaces of computed points and the vertices are used as continuation directions. As new points are computed, the polygons are updated to define new directions. Henderson proves that the continuation provides coverage of the entire family given that the size of the continuation step (i. e. the magnitude of \bar{s}) is small relative to the curvature of the solution surface. In this work, Henderson's curvature condition is not checked explicitly, but the step size is controlled heuristically based on the number of Newton iterations it takes to converge. Leveraging this algorithm to construct families of trajectories ensures that all solutions within the family are dynamically linked, i.e., they are constrained using Equation (10) to be on the same smooth manifold and thus allows each abort family to be uniquely classified.

ABORT INITIAL GUESS CONSTRUCTION PROCESS

Initial guesses for abort trajectories are constructed in the Earth-Moon CR3BP. First, an initial set of trajectory segments are constructed using periapsis Poincaré maps in the Deep Space Trajectory Explorer (DSTE) software tool.^{20–23} The process of constructing these segments is to understand what trajectory geometries exist that may serve as a viable abort. First, an initial trajectory or set of initial trajectories that have unique geometries are constructed in the CR3BP using a series of Poincaré maps. One of these initial trajectories is then used to seed a targeting problem that targets the local minimum impulsive Δv solution in the CR3BP. Once the individual local minimum Δv solution is converged, it is used to seed a multi-parameter continuation scheme to find the family of locally optimal solutions that possess similar characteristics. 18,24 Lastly, these initial guesses are stored according to their time-of-flight and abort Δv_1 time of ignition (TIG). The time-of-flight and TIG information is ultimately used when selecting the proper initial guess to transition to a higher-fidelity model. This investigation focuses on aborts that are initiated after TLI, but before arrival in the NRHO, including aborts where an NRI burn is not executed. This outbound section of the mission is challenging from an abort perspective for several reasons. First, the crew are departing away from the Earth and the propellant cost to "turn around" immediately is high. Second, depending on the type of anomaly that requires an abort to Earth, the crew may have limited life support systems and may not be able to utilitize HLS or Gateway to extend life support before returning to Earth. Lastly, the regions near OPF, beyond OPF and up through NRI are dynamically senstive. Once Orion performs the OPF burn, the spacecraft is moving nearly perpendicular to the Earth-Moon plane at a high energy, which is not a preferential geometry from the perspective of an abort to Earth. Subsequently, nearly all direct-to-Earth aborts that are constructed near this region of the trajectory require a return powered flyby with a low perilune altitude to be within the propellant budget of the Orion vehicle. Conversely, since the Orion capsule will not have performed any other major maneuver, other than OPF and TLI before reaching the NRHO, the majority of the propellant onboard will still be available in the event of an abort. The abort generation techniques are applicable to a range of phases of the mission; however, aborts to Earth that occur while the crew is in the NRHO are going to be the topic of a future investigation.

Constructing the Seed Trajectory in the CR3BP

To build out a family/set of initial guesses, an initial trajectory or set of trajectories must be constructed in the CR3BP to seed the multi-parameter contination process. The process to construct a seed trajectory depends on where along the reference trajectory the abort is initiated, as certain abort geometries are going to be more effective during different phases. Also, it is advantageous to construct various seed trajectories that have different characteristics for a given section of the reference. By having a variety of seed trajectories along a given reference section, a more complete picture of the solution space is understood when the families of initial guesses are fully constructed. A variety of sets/families of initial guesses for a given section of the reference trajectory provides flexibility if unforseen constraints arise when the abort is declared, for example, an anomaly reducing the performance of the propulsion system. The seed trajectories are constructed using periapsis Poincaré maps, which have been effectively leveraged by previous researchers for trajectory design in multi-body systems. Since the transit time between TLI and NRI can vary between 5-11 days depending on the launch opportunity, a reference trajectory is selected that approximately represents the mean possible transit times, i.e., an approximately 8-day transit. Next, that reference trajectory is transformed into a set of non-dimensional states in the Earth-Moon rotating frame. This reference trajectory in the Earth-Moon rotating frame serves as the reference from which all of the aborts are constructed in the CR3BP.

TLI to OPF Abort Initial Guesses

The segment between TLI and OPF encompasses the transit from Earth orbit to the powered flyby by the Moon, i.e., the blue segment labeled "Outbound Transit" in Figure 1. One-burn and two-burn abort strategies are used during this section of reference trajectory. To generate a single burn abort seed trajectory, an Earth-centered periapsis Poincaré map is leveraged in the Earth-Moon CR3BP. First, at each of the discretized states that comprises the reference trajectory, a range of maneuver directions and magnitudes are applied and those states are propagated forward for 14 days. An example of how a trajectory is discretized in the DSTE in the Earth-Moon rotating frame is rendered in Figure 3(a). Trajectories whose first perigee encountered is above 6578 km are removed along with trajectories that do not possess a perigee within the 14 day timepsan. Three example remaining trajectories are rendered in the DSTE in the Earth-Moon rotating frame in green along with the example reference trajectory (red) in Figure 2(a). The green dots indicate where the abort burn is initiated along the reference trajectory. These single-burn trajectories can also be modified with a second maneuver to increase the flexibility to satisfy entry interface conditions.

As the vehicle gets close to the OPF maneuver along the reference trajectory, the dynamics get more sensitive and require alternate strategies. This class of abort trajectory leverages two lunar flybys to return to Earth at a relatively low Δv cost. These are similar to backflip orbits constructed by previous researchers. ^{29–31} An example of this trajectory is rendered in Figure 2(b). To generate a backflip seed trajectory, an Earth-centered periapsis map was also used. Similarly to the trajectories constructed in Figure 2(a), the reference trajectory is discretized and maneuvers are applied in a variety of directions and magnitudes between 1 and 300 m/s. the section of the trajectory that is discretized is just before OPF, where the dynamics begin to get more sensitive due to lunar gravity. To isolate the backflip orbits, the discretized states with Δv 's applied are propagated for 30 days and the second perigee encountered is checked to ensure that it is within a 10,000 km radius of the Earth. These criteria filter out trajectories similar to those found in Figure 2(a), while keeping the trajectories with a backflip geometry. The ballistic backflip abort trajectory rendered in Figure 2(b) is an example of single-burn abort; however, additional maneuvers can be include, such as at the second lunar flyby, to make it a two-burn solution and potentially reduce the overall maneuver cost.

OPF to NRI Abort Initial Guesses

The segment along the reference trajectory from OPF to NRI presents more challenges given the energy and direction of the segment. For example, consider the trajectory segment between OPF and NRI from Figure 1. The Deep Space Trajectory Explorer (DSTE), a multi-body trajectory design software tool, is used

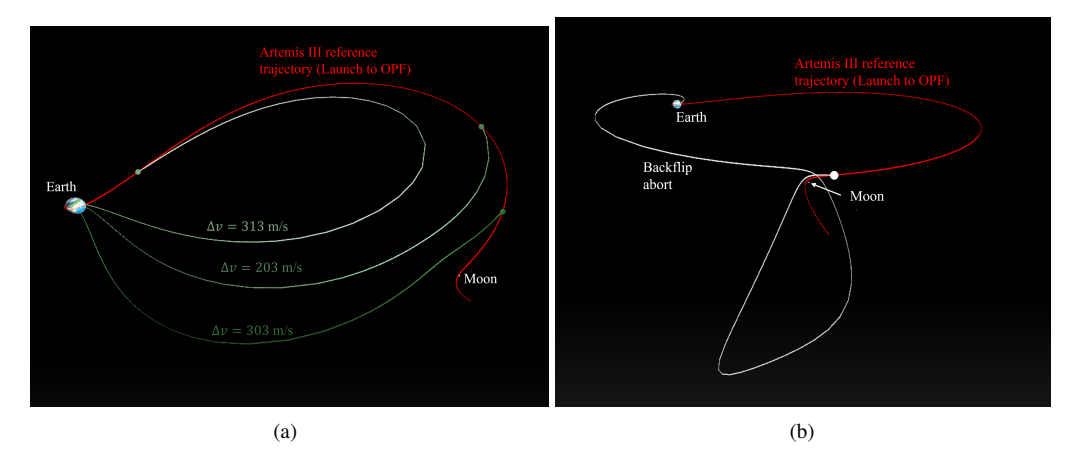


Figure 2. (a) Three TLI to OPF abort initial guess trajectories that leverage one burn to return to Earth. (b) Backflip abort example in the CR3BP (the white dot indicates the start of the abort). All trajectories are rendered in DSTE in the Earth-Moon rotating frame.

to find these initial segments. Generally, for this OPF to NRI phase of the mission, a low-altitude, powered flyby of the Moon is required to leverage the Oberth effect and reduce Δv costs. Subsequently, the first abort maneuver attempts to change the energy of the trajectory such that the next periapsis is at a low altitude. Additionally, the velocity vector at the flyby must be in the -y direction in the Earth-Moon rotating frame such that a possible return-to-Earth segment is aligned properly. Following these two criteria, potential trajectory arcs are constructed using a periapsis Poincaré map. The OPF to NRI trajectory segment is discretized into a set of states along the segment, and a range of maneuver directions and magnitudes (between 1 and 700 m/s) are applied to each of the states. The states are then propagated forward for 14 days and trajectories that have a perilune radii below 10,000 km radius are recorded. Three trajectory arcs are rendered in Figure 3(b) in the Earth-Moon rotating frame in DSTE that attempt to characterize the dominant trajectory geometries, label Abort arc A, B, and C. The colored dots in Figure 3(b) correspond to the departure location off of the reference trajectory (red). Two of the geometries (Abort arcs A and B) possess perilunes over the north pole of the Moon, while the third trajectory geometry (Abort arc C) possesses a perilune over the south pole of the Moon. Using the final perilune state along each of these three segments, another maneuver is applied and propagated until reaching a perigee within 50,000 km of the Earth. This second segment serves as initial guess for the return powered flyby (RPF) to entry interface segment to complete the Earth-return abort. Information from these two segments is used to construct a constrained, feasible trajectory in the CR3BP.

ABORT TRAJECTORY FAMILIES

Construction of an initial seed trajectory in the CR3BP ultimately serves to feed a continuation/optimization method described in the previous section to develop a family of abort trajectories. One-, two-, and three-burn abort families are constructed using these seed trajectories and ultimately serve as the initial guesses for transition to higher fidelity. For all of the cases, a representation of the reference trajectory needs to be included in the targeting problem. Subsequently, a spline over the 8-day transit reference trajectory, used previously to generate the seed trajectories, is constructed which provides a function that takes in non-dimensional time along the reference and returns the 6-element state at that time along the reference. Splining provides a smooth, differentiable function representation of the reference trajectory such that first node of the abort trajectory can be constrained anywhere along the selected reference. Families of one-burn aborts are constructed between TLI and OPF, as well as families of backflip orbits within this section of the reference trajectory. For aborts that occur post-OPF, two-burn and three-burn abort families are constructed and compared.

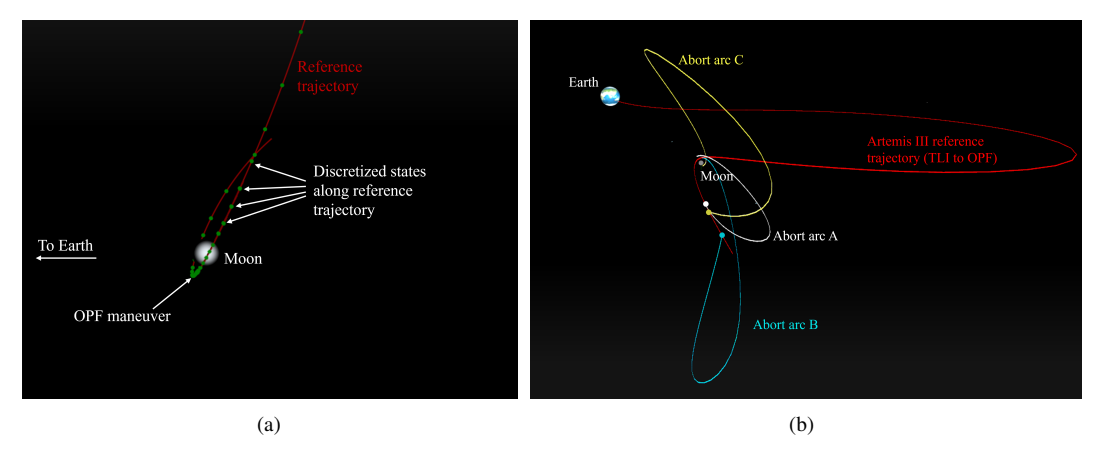


Figure 3. (a) Discretized reference trajectory to create the initial conditions that generate a periapsis Poincaré map in the DSTE. The section of the reference shown is approaching OPF and the segment between OPF and NRI, rendered in the Earth-Moon rotating frame. (b) Three arcs that encounter a low perilune after the first Δv is initiated.

TLI to OPF Abort Families

Two classes of aborts are investigated for the section of the reference trajectory between the TLI and OPF maneuvers, First, families of one-burn return aborts are constructed from TLI to OPF. For one-burn aborts, a single Δv is performed to return the vehicle back to the Earth entry conditions. One-burn abort generally possess a higher Δv than an equivalent two-burn abort, but they are preferred from an operational perspective since only a single deterministic maneuver is required. Free-variable and constraint vectors for a one-burn abort are defined,

$$\bar{X} = \begin{bmatrix} \Delta \bar{v}_{1} \\ \bar{x}_{1}^{+} \\ \bar{x}_{2}^{-} \\ t_{1} \\ \beta_{t_{\text{ref, min}}} \\ \beta_{t_{\text{ref, min}}} \\ t_{\text{ref}} \\ t_{\text{abort}} \end{bmatrix} \qquad \bar{F} = \begin{bmatrix} \sin(\gamma) - \frac{\bar{r}_{2} \cdot \bar{v}_{2}^{-}}{||\bar{r}_{2}^{-}|| \cdot ||\bar{v}_{2}^{-}||} \\ ||\bar{r}_{1}^{-} - \bar{r}_{\text{ref}}(t_{\text{ref}}) \\ \bar{v}_{1} - (\bar{v}_{\text{ref}}(t_{\text{ref}}) + \Delta \bar{v}_{1}) \\ \bar{x}_{2}^{-}(-\frac{t_{1}}{2}) - \bar{x}_{1}^{+}(\frac{t_{1}}{2}) \\ t_{\text{abort}} - t_{1} \\ t_{\text{ref}} - t_{\text{ref, max}} + \beta_{t_{\text{ref, max}}}^{2} \\ t_{\text{ref}} - t_{\text{ref, min}} - \beta_{t_{\text{ref, min}}}^{2} \end{bmatrix}$$

$$(12)$$

where Δv_1 is the impulsive abort maneuver, \bar{x}_1^+ is the post-abort maneuver state, \bar{x}_2^- is the final state along the abort trajectory, t_1 is the abort time-of-flight, and $\beta_{t_{\rm ref, max}}$ and $\beta_{t_{\rm ref, min}}$ are slack variables that bound the time along the reference between $t_{\rm ref, min}$ and $t_{\rm ref, max}$, which are approximately 12 hours and 8.5 days after launch, respectively. In the constraint vector, $\gamma = -5.8^\circ$, which is the flight path angle at the end of the abort trajectory, $h_{\rm EI} = 122\,{\rm km}$ is the altitude at the end of the trajectory, $\bar{r}_{\rm ref}(t_{\rm ref})$ and $\bar{v}_{\rm ref}(t_{\rm ref})$ are the position and velocity along the reference trajectory at $t_{\rm ref}$, and $t_{\rm abort}$ is the desired abort time of flight. The graphic in Figure 4 illustrates an example of a one-burn abort targeting problem. Using the seed trajectory from Figure 2(a) corresponding to 303 m/s, a family of locally optimal Δv trajectories is constructed, where the cost function is the magnitude of the Δv . Examples of one-burn aborts as well as the Δv as a function of time-of-flight and time of ignition (TIG) along the reference for the abort maneuver are plotted in Figure 5. The colored dots on the left side correspond to the location of the abort maneuver along the reference trajectory (black) and the numbers next to those dots correspond to where on the Δv plot the abort trajectory is represented. Two families are classified in the set of one-burn aborts, where the upper section of the Δv plot on the right in Figure 5 corresponds to trajectories that have perilunes on the far side of the Moon. The remaining trajectories

possess perilunes that are on the near side of the Moon relative to the Earth. While these examples are not the only one-burn aborts initial guesses available, they provide insight into the dynamics when a single abort maneuver is allowed.

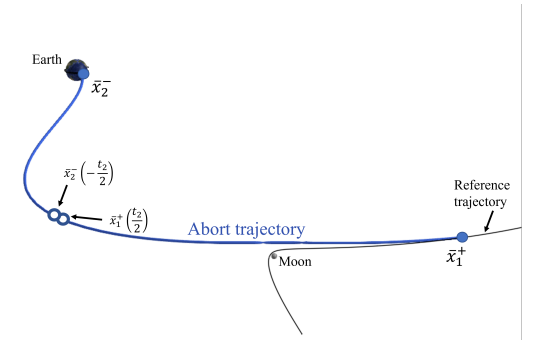


Figure 4. One burn abort targeting scheme. The closed circles represent the start of a trajectory segment and the open circles represent the end of a trajectory segment.

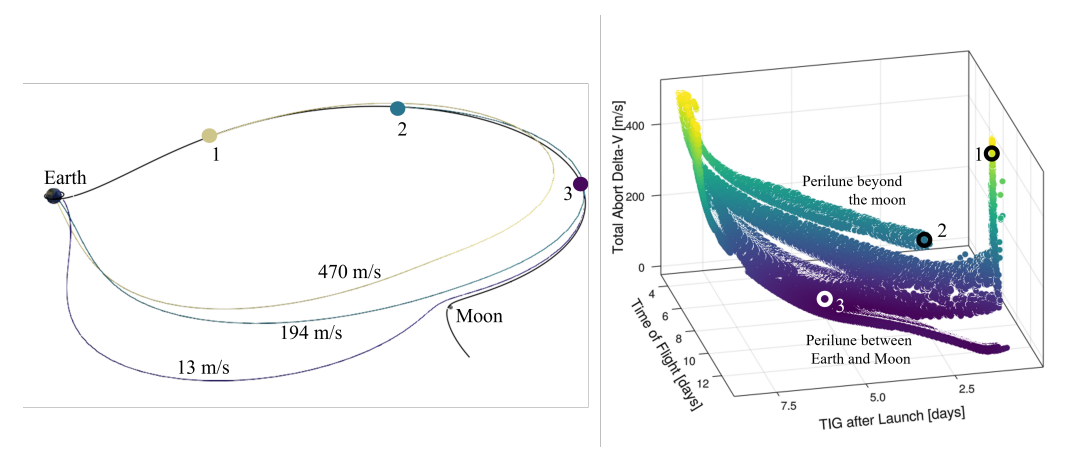


Figure 5. Examples of one-burn aborts (left) and the abort Δv as a function of time of flight and abort maneuver TIG (right).

The one-burn aborts that have been constructed in Figure 5 generally remain near the Earth-Moon plane. However, as demonstrated in Figure 2(b), there is a class of trajectories that leverage two lunar flybys and extend below the Earth-Moon plane. This class of trajectories are denoted backflip aborts, as they are similar to backflip orbits studied in previous investigations. $^{29-31}$ The backflip aborts are generally more Δv efficient as the vehicle approaches the OPF maneuver near the Moon, where the Δv required for one-burn aborts from Figure 5 begins to increase substantially. When considering a backflip abort, the segment between each of the lunar flybys generally takes around 14 days, since the vehicle's orbit is in nearly a 1:1 resonance with the Moon. Given the longer time-of-flight, this class of aborts is generally only feasible for shorter outbound transits along the reference trajectory. Additionally, while the seed ballistic backflip abort trajectory rendered in Figure 2(b) is an example of single-burn abort, additional maneuvers are included to expand the solution space. Specifically, two-burn and three-burn variations of this backflip orbit have been investigated as potential abort trajectory families. In the two-burn case, the second burn is placed about halfway between the first perilune flyby and apolune, approximately 3.6 days after the first burn. This solution requires a total of 89 m/s of Δv and has a 22-day time-of-flight. To generate a family of return trajectories leveraging this solution, a multiple-shooting and natural parameter continuation scheme is implemented. This continuation scheme aims to produce a family of returns with lower times-of-flight. The free-variable vector contains the Δv components of the two maneuvers, as well as the times-of-flight of the two abort arcs: the arc between the first abort Δv and the second abort Δv , and the arc between the second abort Δv and the return to Earth. The total time of flight, however, is constrained; after the differential corrector delivers a solution, the time-of-flight of the next solution is decremented by a small amount (18 minutes) and converged using the previous solution as an initial guess. There is also a constraint on the Earth distance at the end of the second abort arc. This constraint ensures only that the abort trajectory returns to Earth, i.e., it does not specify a particular location on the surface and the return distance is constrained to 6528 km. Finally, the multiple-shootering scheme includes constraints enforcing continuity between segments; the first arc is split into two segments, and the second arc is split into four segments.

The results of this continuation process are shown in Figure 6. The total time of flight was reduced from 22 days to 19 days; however, the Δv required to shorten the times-of-flight are quite large. At this stage in the continuation process, the differential corrector was not able to converge solutions with fewer than 40 iterations, and due to the large Δv required, analysis efforts focused on a new variation of the backflip abort.

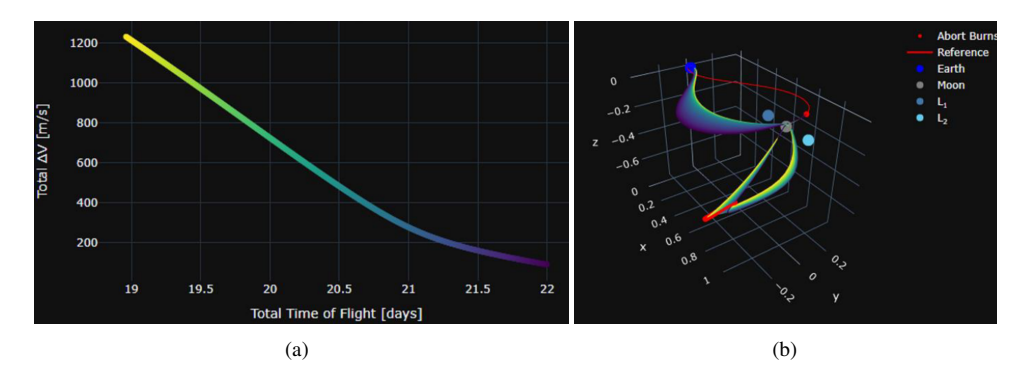


Figure 6. Results of the two-burn backflip abort continuation process. (a) Time of flight and Δv results of each solution (the color axis is identical to the y-axis). (b) Converged abort trajectories in the nondimensional Earth-Moon rotating frame. The colors of the trajectories in (a) map to the marker colors in (b).

A three-burn variation of the backflip orbit was also investigated. This variation placed a burn at the first perilune flyby, between the two existing maneuvers in the two-burn backflip returns. A similar natural parameter continuation strategy was implemented, with the burn components and timing of the perilune burn added to the free-variable vector. The time decrement between solutions is increased to 80 minutes. Further, the continuation process was amended with a 1 m/s velocity increment to the flyby burn applied at subsequent solutions of the continuation process. This increment was added because preliminary testing indicated that increasing velocity at perilune resulted in shorter times of flight. The results are plotted in Figure 7. As with the two-burn variation, even small improvements to the overall time of flight require large maneuvers. This continuation process was stopped after a time of flight decrease of about 1.5 days due to hitting iteration limits in the differential corrector as well as the large maneuver cost. Generally, given the longer times-of-flight for the backflip aborts, they tend to violate the limit for available consumables onboard the Orion crew capsule. However, understanding the characeteristics of the backflip aborts provides a more complete picture of the available options if an anomaly occurs.

Post-OPF Abort Families

After the outbound powered flyby maneuver is executed along the reference trajectory, the vehicle follows a path out of the Earth-Moon plane until the NRHO insertion maneuver. This section of the reference trajectory is a challenging region to design aborts because the vehicle is moving away from the Moon at high energy, nearly perpendicular to the Earth-Moon plane, and after two major maneuvers, TLI and OPF, have been executed. However, various abort options are constructed that leverage a lunar flyby to return to Earth. First, a two-burn abort is investigated that leverages the cislunar dynamics that, after the first abort maneuver, bends the trajectory back towards a flyby over the south pole of the Moon. An example of one of these trajectories

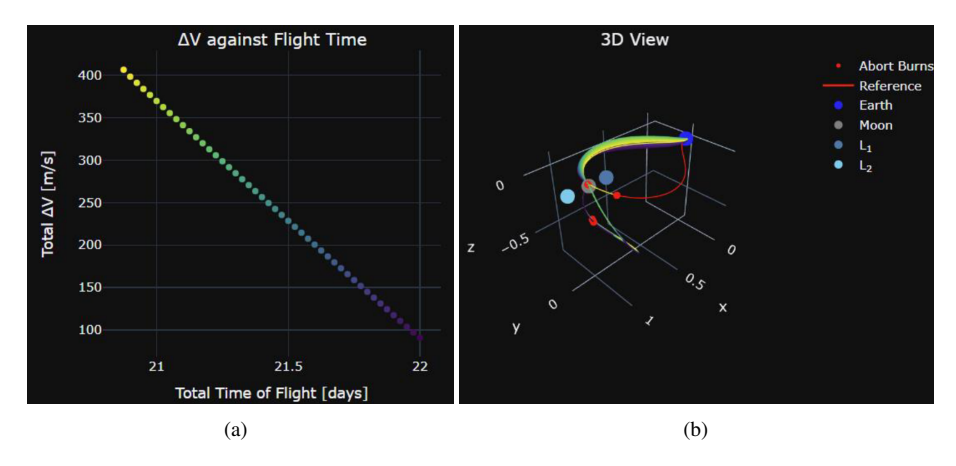


Figure 7. Results of the three-burn backflip abort continuation process. (a) Time of flight and Δv of each solution (the color axis is identical to the y-axis). (b) Converged abort trajectories in the nondimensional Earth-Moon rotating frame. The colors of the trajectories in (a) map to the marker colors in (b).

is rendered in Figure 9(a) using the seed trajectory constructed in the DSTE from abort arc C in Figure 3(b). A set of free-variables, \bar{X} , constraints, \bar{F} and cost function, J, are defined for this two-burn abort,

$$\bar{X} = \begin{bmatrix} \Delta \bar{v}_{1} \\ \Delta v_{2} \\ t_{1} \\ t_{2} \\ \bar{x}_{1} \\ \bar{x}_{2}^{-} \\ \bar{x}_{3}^{-} \\ \beta_{t_{\text{ref, min}}} \\ \beta_{\text{alt, min}} \\ t_{\text{ref}} \\ t_{\text{abort}} \end{bmatrix} \qquad \bar{F} = \begin{bmatrix} \sin(\gamma) - \frac{\bar{r}_{3} \cdot \bar{v}_{3}}{||\bar{r}_{3}|| \cdot ||\bar{v}_{3}||} \\ ||\bar{r}_{3}|| - h_{\text{EI}} \\ \bar{r}_{1} - \bar{r}_{\text{ref}}(t_{\text{ref}}) \\ \bar{v}_{1} - (\bar{v}_{\text{ref}}(t_{\text{ref}}) + \Delta \bar{v}_{1}) \\ \bar{r}_{2}^{+} - \bar{r}_{2}^{-} \\ \bar{v}_{2}^{+} - \bar{v}_{2}^{-} + \Delta v_{2} \hat{v}_{2}^{-} \\ \bar{v}_{2}^{+} - \bar{v}_{2}^{-} + \Delta v_{2} \hat{v}_{2}^{-} \\ \bar{x}_{2}^{-} (-\frac{t_{1}}{2}) - \bar{x}_{1} (\frac{t_{1}}{2}) \\ \bar{x}_{3} (-\frac{t_{2}}{2}) - \bar{x}_{2}^{+} (\frac{t_{2}}{2}) \\ \bar{r}_{2}^{-} \cdot \bar{v}_{2}^{-} \\ t_{\text{abort}} - (t_{1} + t_{2}) \\ t_{\text{ref}} - t_{\text{ref, max}} + \beta_{t_{\text{ref, min}}}^{2} \\ t_{\text{ref}} - t_{\text{ref, min}} - \beta_{t_{\text{ref, min}}}^{2} \\ ||\bar{r}_{2}^{-}|| - h_{\Delta v_{2}} - \beta_{\text{alt, min}}^{2} \end{bmatrix}$$

$$(13)$$

where $\Delta \bar{v}_1$ and Δv_2 are the abort maneuvers, t_1 is the time-of-flight from the first abort burn to the second abort burn, t_2 is the time-of-flight from the second abort burn to the Earth entry state, x_1 is the post- $\Delta \bar{v}_1$ state, \bar{x}_2^- is the pre- $\Delta \bar{v}_2$ state, \bar{x}_2^+ is the post- $\Delta \bar{v}_2$ state, \bar{x}_3^- is the Earth-entry state, and $\beta_{t_{\mathrm{ref,\,max}}}$ and $\beta_{t_{\mathrm{ref,\,min}}}$ are the slack variables that bounding the segment of the reference trajectory that the abort is initiated along, $\beta_{\rm alt,\ min}$ is a slack variable for the minimum altitude at the second abort burn, and $t_{\rm ref}$ is the time along the reference trajectory that the first abort maneuver is initiated. Within the constraint vector, t_{abort} is the desired timeof-flight of the abort, γ is the flight path angle at entry interface of the abort trajectory, defined as -5.8° in this investigation, $h_{\rm EI}$ is the desired altitude at entry interface, $||\bar{r}_3||$ is the Earth-centered position magnitude at entry interface, \bar{r}_i and \bar{v}_i are the position and velocity components of the state \bar{x}_i , respectively, $\bar{r}_{\rm ref}(t_{\rm ref})$ and $\bar{v}_{ref}(t_{ref})$ are the position and velocity along the reference trajectory, respectively, at t_{ref} , $\bar{x}_i(t)$ is the state \bar{x}_i propagated in the CR3BP for time t, $t_{\text{ref, max}}$ and $t_{\text{ref, min}}$ are the minimum and maximum times along the reference trajectory that first abort maneuver is allowed to occur, $h_{\Delta v_2}$ is the minimum altitude that Δv_2 is allowed to occur, and \hat{v}_2^- is the velocity direction at \bar{x}_2^- . Higher-fidelity in-space abort trajectories require the final state to be constrained to a horizontal and vertical target line; however, to ensure that initial guess trajectories are launch and return epoch agnostic, only a subset of the target line constraints are imposed. These constraints included in the initial guess are the approximate flight path angle and altitude. 32 A diagram of the targeting process is illustrated in Figure 9(a). Also note that the two-burn targeting example includes an altitude constraint. For the two-burn abort geometry constructed in this investigation, the maneuver cost is driven down by how low the lunar flyby altitude is at \bar{x}_2 ; therefore, a slack variable, $\beta_{\rm alt, \, min}$, is included to prevent solutions from passing below 100 km altitude from the lunar surface.

Using the targeting problem defined in Equation (13) paried with optimization and multi-parameter continuation from Equation (11), families of two-burn aborts are generated. The total abort cost as a function of the abort time-of-flight and TIG after OPF is plotted on the right in Figure 8. Note that there are two surfaces of solutions in the Δv plot in Figure 8. The top surface represents aborts that possesses a final state that is descending, i.e., the z-component of velocity is negative at the final state, and the bottom surface represents aborts that have a final state that is ascending, i.e., the z-component of velocity is positive. Examples of two-burn aborts are rendered on the left in Figure 8, where colored dot represents the location along the reference trajectory where the first abort maneuver is executed. The number next to each of the dots corresponds to where the associated trajectory is in the Δv plot on the right in Figure 8. These families of two-burn aborts also appear to incorporate motion similar to the stable/unstable manifolds of the L_2 axial orbits or L_2 Lissajous orbits. Also note that there are no abort trajectories with a less than 10.7 day time of flight, which limits the feasibility of this type of abort geometry given the crew life support system constraint of 21 days. These generally are feasible for reference trajectories that have shorter transit times.

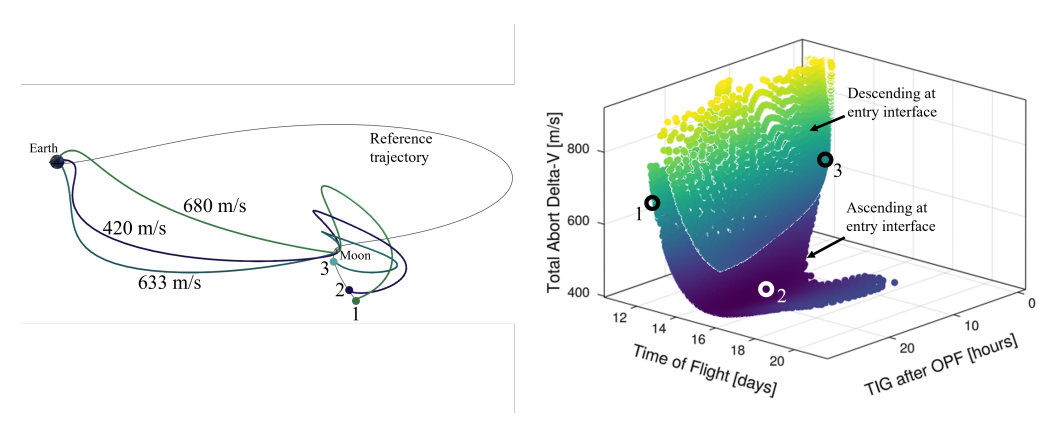


Figure 8. Examples of two-burn aborts (left) and the abort Δv as a function of time of flight and abort maneuver TIG (right).

In the post-OPF region of the trajectory, three-burn abort families that are constructed using the seed abort arcs A and B are rendered in Figure 3(b). While there are classes of these trajectories that exist as two-burn solutions, a third maneuver is included in the targeting problem to increase flexibility for these types of aborts. For abort arc A and B from Figure 3(b), a maneuver is allowed at apolune of those arcs, but the manuever direction is constrained such that it is perpendicular to the Moon-centered position vector. This constraint allows the maneuver to be strictly a plane change maneuver at apolune to provide the correct orientation of the orbit plane before the final powered lunar flyby to return to Earth. For the three-burn aborts in the

post-OPF region, the set of free-variables, constraints, and cost function, J, are defined,

$$\bar{X} = \begin{bmatrix} \Delta \bar{v}_{1} \\ \Delta \bar{v}_{2} \\ \Delta v_{3} \\ t_{1} \\ t_{2} \\ t_{3} \\ \beta_{t_{\text{ref, max}}} \\ \beta_{t_{\text{ref, min}}} \\ t_{\text{ref}} \\ t_{\text{abort}} \end{bmatrix} \qquad \bar{F} = \begin{bmatrix} \sin(\gamma) - \frac{\bar{d}_{3}(t_{3}) \cdot \bar{v}_{3}(t_{3})}{||\bar{d}_{3}(t_{3})|| \cdot ||\bar{v}_{3}(t_{3})||} \\ ||\bar{d}_{3}(t_{3})|| - h_{\text{EI}} \\ \bar{r}_{1}(t_{1}) \cdot \bar{v}_{1}(t_{1}) \\ \bar{r}_{2} \cdot \bar{v}_{2} \\ \bar{r}_{1}(t_{1}) - \bar{r}_{2} \\ \bar{v}_{1}(t_{1}) + \Delta \bar{v}_{2} - \bar{v}_{2} \\ \bar{r}_{2}(t_{2}) - \bar{r}_{3} \\ \bar{v}_{2}(t_{2}) + \Delta v_{3}\hat{v}_{2}(t_{2}) - \bar{v}_{3} \\ t_{1} + t_{2} + t_{3} - t_{\text{abort}} \end{bmatrix}$$

$$J = ||\Delta \bar{v}_{1}|| + ||\Delta \bar{v}_{2}|| + |\Delta v_{3}|$$
 (14)

where \bar{x}_2 and \bar{x}_3 are the states after the second and third maneuvers, $\Delta \bar{v}_1$ and $\Delta \bar{v}_2$ are the first two maneuver vectors, Δv_3 is maneuver mangitude of the third maneuver, t_i is the time-of-flight of the i^{th} segment, and \bar{r}_i is the Moon-centered position associated with \bar{x}_i , \bar{v}_i is the velocity associated with state \bar{x}_i , \bar{d}_i is the Earth-centered position vector associated with state \bar{x}_i and $\bar{x}(t_i)_i$ is the state after \bar{x}_i is propagated for time t_i . Note that an apse is constrained before and after the second maneuver. These two constraints enforce Δv_2 to be perpendicular to the Moon-centered position vector, i.e., the maneuver can change the plane and/or increase/decrease the energy of the trajectory only. A diagram of the targeting problem is illustrated in Figure 9(b). The three-burn targeting problem also only leverages forward shooting, as compared to forward/backward shooting for the one-burn and two-burn aborts. This convention was selected to reduce the number of free-variables and constraints to decrease runtime when generating the families of aborts.

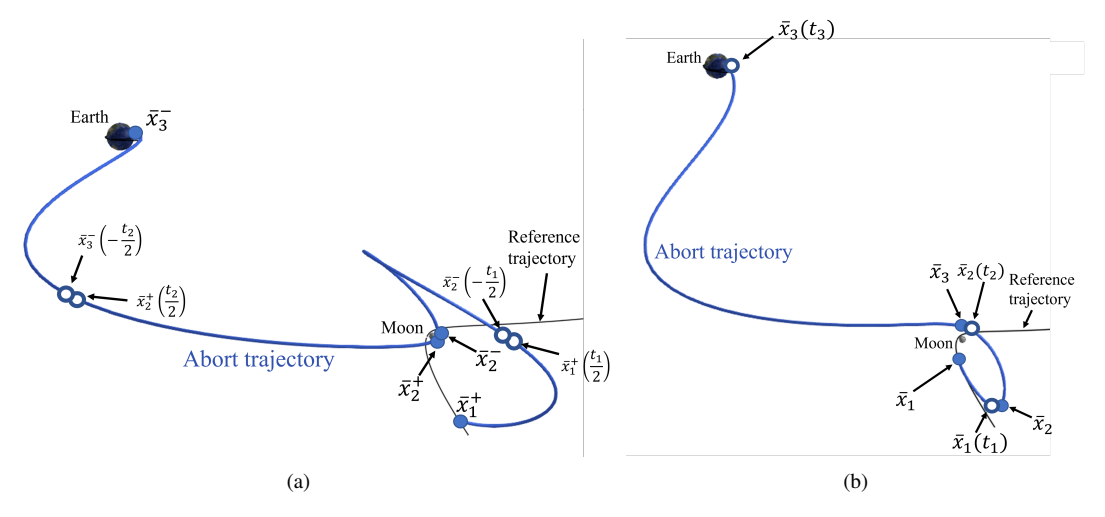


Figure 9. (a) Two burn abort targeting scheme. (b) Three-burn abort targeting scheme. The closed circles represent the start of a trajectory segment and the open circles represent the end of a trajectory segment.

The targeting problem defined in Equation (14) is paired with the multi-parameter continuation process to generate families of two different three-burn abort families. The total abort Δv is plotted as a function of abort time-of-flight and the $\Delta \bar{v}_1$ TIG relative to OPF for each family in Figures 10 and 11. The family generated using the seed trajectory associated with abort arc A in Figure 3(b) is defined as Family A and the family that is generated using abort arc B is defined as Family B. Family A is characterized by Δv_1 generally being in the anti-velocity direction and times of flight less than 12 days. The family is only generated for TIGs

up to 48 hours after OPF. Three examples of abort trajectories from Family A are plotted on the left in Figure 10, also zooming in to show the region near the Moon. The example trajectories evolve as the TIG after OPF increases, where the plane change imparted by Δv_2 at apolune of all of the aborts is more noticeable for example 2 and 3. The colored arrows in the zoomed in view in Figure 10 indicate the direction of motion of the trajectory. The red region in Figure 10 indicates TIGs that occur after NRI, i.e. post-NRI. These trajectories in the post-NRI region serve as initial guesses in the event of a missed-NRI burn. Similar data is plotted after Family B is constructed in Figure 11(a), where two perspectives of the same data are shown. The post-NRI region is highlighted in red and several example abort trajectories are plotted in Figure 11(b). The integer number next to the Δv value indicates how the trajectories correspond in the zoomed view. Note that surface of solutions in Family B wraps around such that there is more than one solution for a given combination of time-of-flight and Δv_1 TIG. Trajectories 1 and 2 in Figure 11(b) represent solutions that possess nearly the same Δv and the same time-of-flight, but have TIGs at different times, where solution 2 is on the back side of perspective of the surface shown on the right in Figure 11(a). These two trajectories possess different behavior in the vicinity of the Moon. The apolune of solution 1 is at a higher altitude than the apolune of solution 2, and the plane change is more significant in solution 2 at apolune than in solution 1. Family B, compared to Family A, is characterized by the first abort maneuver having a significant component in the -y-direction, causing trajectory to travel nearly perpendicular to the Earth-Moon plane after Δv_1 . Family B also generally has longer times-of-flight than Family A and there are no solutions in Family B that have time-of-flight less than 12 days. Family A and B combined cover a significant set of the time-of-flight/TIG space, providing an understanding of potential abort options for the region after the OPF maneuver.

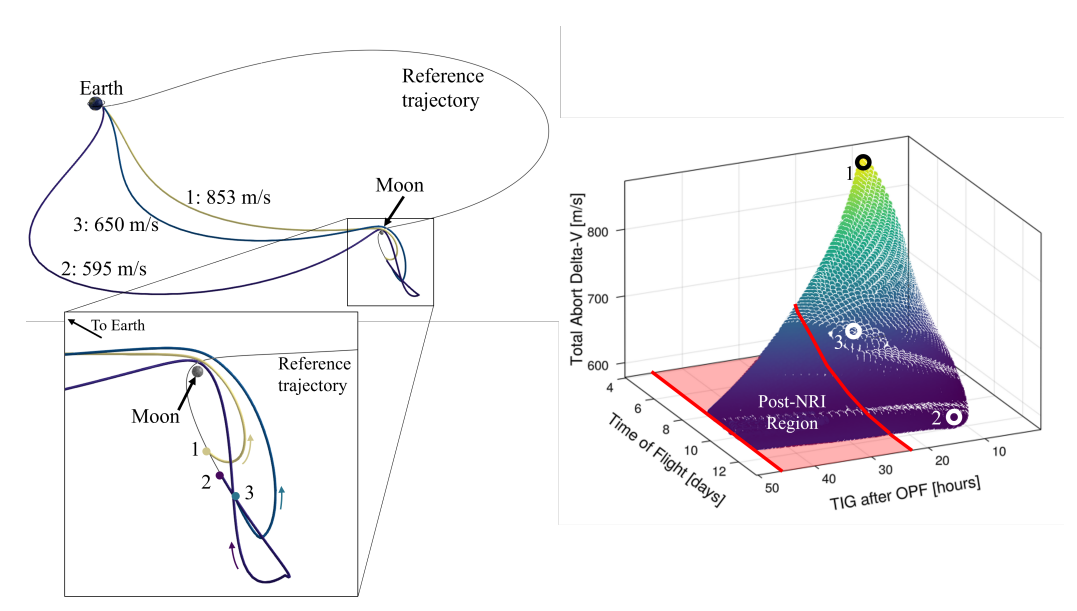


Figure 10. Family A three-burn abort family. Example trajectories are plotted in the Earth-Moon rotating frame on the left and the total abort Δv is plotted as a function of time-of-flight and TIG after OPF. Note that the red line on the Δv plot indicates when the NRI TIG occurs. The trajectories that are constructed in the region with higher TIGs than the NRI TIG can be leveraged in the case of a missed NRI.

The families of two-burn and three-burn aborts constructed in the CR3BP in this investigation are not the exhaustive set of potential abort geometries. However, given the methods used to construct these aborts, they provide a broad understanding of some of the dominant motion in the region. To visualize how all of these families compare to one another, the Δv as a function of time-of-flight and TIG are plotted for all of the post-OPF families in Figure 12. Note that all of the families possess solutions with times-of-flight of 12 days; thus, multiple initial guesses can be delivered to from the same TIG after OPF to return the crew to Earth. The ability to have multiple abort options for a given TIG/time-of-flight combination provides flexibility in the event that one of the initial guesses fails to converge in the higher-fidelity model, an eclipse occurs along

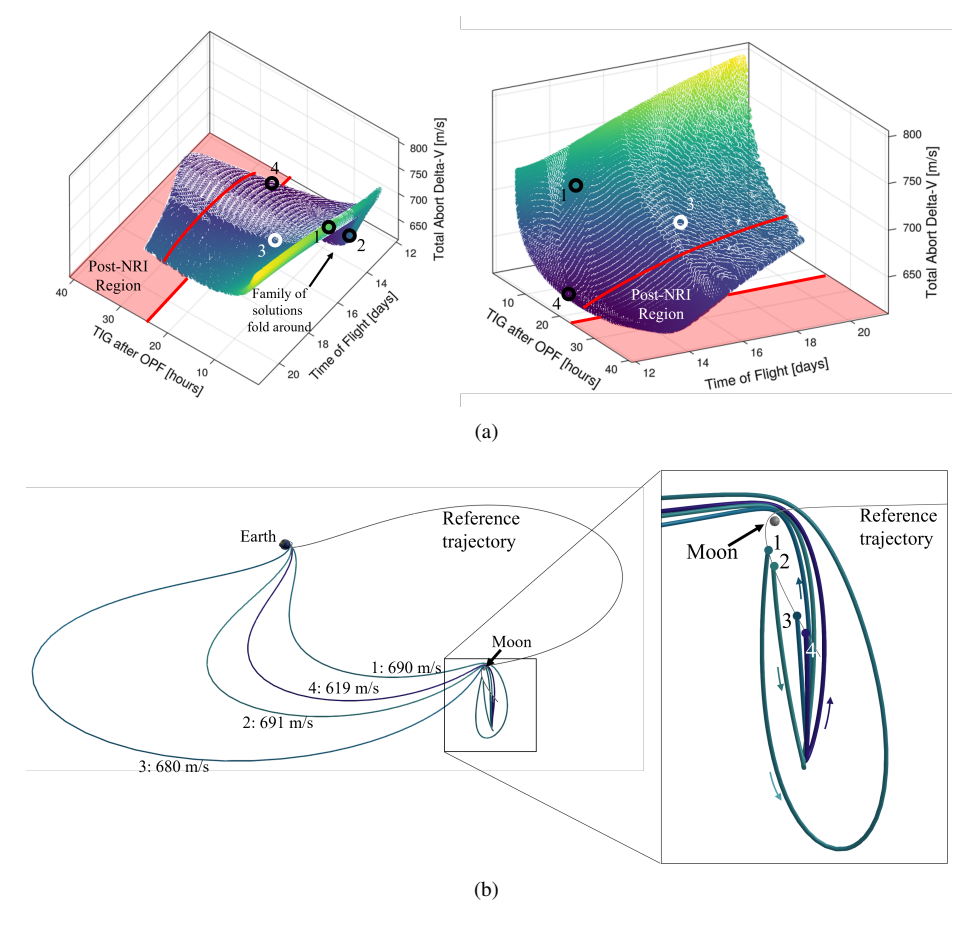


Figure 11. (a) Two perspectives of Δv plotted as a function of time-of-flight and the first abort burn TIG for Family B (b) Four examples of abort trajectories from Family B. Note the integer next to the Δv value in the view on the left indicates what corresponds in the zoomed in view on the right.

a particular abort trajectory, or that there is an anomaly preventing the ability to execute one of the abort geometries.

TRANSCRIPTION AND CONVERGENCE IN HIGHER-FIDELITY

Effective methods to generate initial guesses are ultimately required to seed a higher-fidelity optimization process. The CR3BP provides insight into the fundamental motion in the Earth-Moon vicinity. However, the higher-fidelity convergence process is also critical to ensure that an initial guess trajectory persists in a model that more accurately represents the dynamics that are experienced during the mission. In this investigation, a process is summarized that describes the transition from the Earth-Moon CR3BP to a higher fidelity ephemeris model to validate the initial guess solutions constructed. Ultimately, the initial guesses should provide an approximation of the total abort maneuver cost and time-of-flight such that initialition is built before the transition to higher-fidelity, which generally requires more computational resources than initial guess construction.

High-Fidelity Tools – Copernicus and Damocles

The convergence process is conducted using the Copernicus software package. Copernicus is a generalized spacecraft trajectory design and optimization tool^{33,34} capable of producing optimal trajectories with a variety

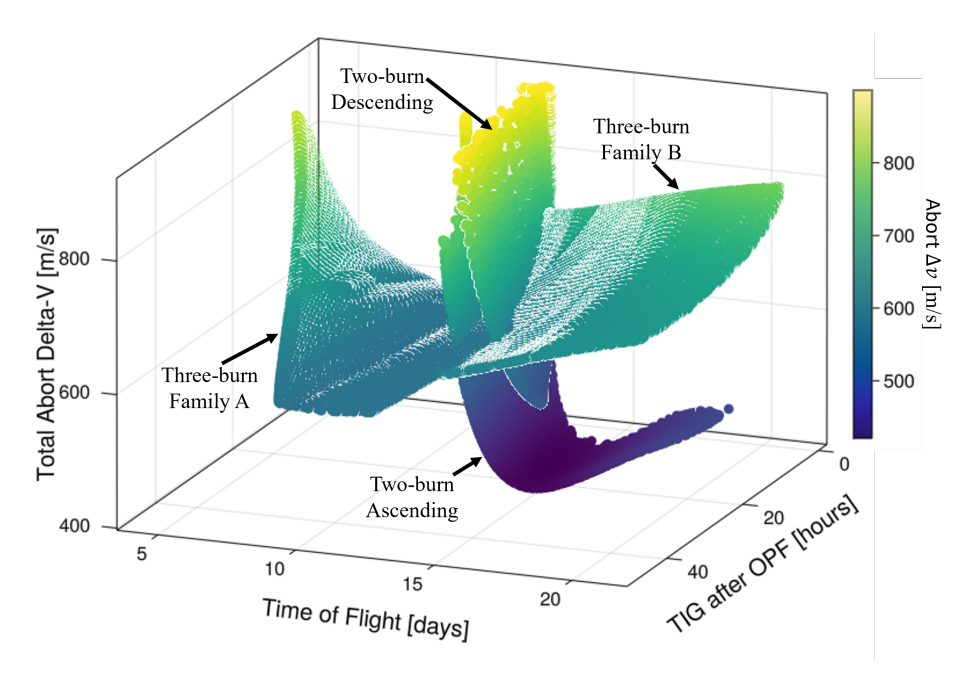


Figure 12. Total abort maneuver costs as a function of time-of-flight and TIG after OPF for the ascending and descending arrival two-burn families and three-burn Family A and B.

of constraints and variety of model fidelities. It was used extensively by the Artemis mission design team to support Artemis I preflight analyses as well as on-console in Mission Control Center (MCC) throughout the 26-day mission. Copernicus continues to be used heavily to support mission design efforts for Artemis II, Artemis III, and Artemis IV+ due to its versatility to handle a wide range of trajectory profiles.

The Artemis mission design team also actively develops and utilizes a package known as Damocles to automate Copernicus optimization tasks. Damocles, a suite of Python-based scripting utilities, allows trajectory "scans" of millions of nominal and off-nominal trajectories to be setup, optimized, and analyzed all in a highly parallelizable and automated fashion.³⁵ These trajectory scans represent individual trajectories as unique nodes in a large Directed Acyclic Graph (DAG) defining the order of dependencies in which trajectories can be converged. This framework ensures that each trajectory, represented by a unique combination of scan parameters of interest, receives a reasonable initial guess for convergence. However, by using an external initial guess process to seed individual nodes, the scan DAG becomes much more parallelizable due to fewer dependencies (i.e., edges) between nodes, thus runtime and convergence can be dramatically improved.

Table 1 provides an example of the various scan parameters used to define individual abort trajectories for an Artemis III Damocles scan. These scan parameters define a highly multi-dimensional subspace of trajectory solutions, with many different possible permutations of these parameters defining unique trajectories. While the number of scan parameters increases the complexity of abort analyses, it provides preflight insights into a vast number of potential abort scenarios and corresponding solution trajectories.

Transcription Process Between Models

Though the initial guess solutions modeled in the CR3BP provide reasonable estimates of abort capabilities, they do not model all system constraints needed to define a feasible full-fidelity abort trajectory profile. For example, the Copernicus/Damocles solutions implement a full polynomial spline defining the set of allowable EI corridor entry states and has discrete time-of-flight constraints for minimum time between abort burns to allow for thermal and operational constraints. A transcription process was developed to transition initial guesses from the CR3BP into higher-fidelity Copernicus models. The transcription process and results

Table 1. Abort scan parameters for Damocles scans

Scan Parameter	Description
Launch Day	Day of launch for "launch period" scans
Launch Time	Epoch of launch for "launch window" scans
Mission Phase	Current phase of the mission timeline in which abort occurs. E.g., "Post-TLI" or "Post-OPF"
Last Nominal Burn Percentage Completed	Percentage of last burn completed for missed/partial burn scenarios. E.g., 0% for a missed-OPF abort, 1-99% for a partial-OPF abort. 100% represents a nominal burn with an abort declared sometime during the coast phase following the burn.
Number of Abort Burns	Number of burns required for the abort profile. Typically 1-3 burns.
Abort Burn Engine	Engine that abort burns occur. Typically OMSe or 8+X (if abort caused by primary engine failure).
Entry Interface (EI) Day	Integer day in which Entry Interface (EI) occurs. E.g., EI = 17 corresponds to an abort trajectory with 16.5 < EI MET < 17.5 days.
Abort Burn 1 (AB1) TIG	Abort Burn 1 (AB1) Time of Ignition (TIG). Defines the point in time in which the abort is officially initiated.
Abort Solution Family	Additional scan parameter to distinguish different dynamical families of solutions.

are also described in detail by Owen et al., but the process is summarized in this paper for completeness.³⁶

An interface between initial guess data and high-fidelity input data was first developed to aid in the transcription process. CR3BP initial guess data was converted to a database of solutions in the standardized data-exchange JavaScript Object Notation (JSON) format. This JSON database contains thousands of individual initial guess profiles, with each profile containing information on abort burn Δv vectors, state vectors at abort burns, and time-of-flights between states. With some state and frame transformations, this data is converted into the set of free-variables, or Optimization Variables (OVs) required by Copernicus, to define the controls of the constrained optimization problem.

Figure 13 details the transcription process for a single trajectory node (i.e., a unique combination of scan parameters from Table 1) within a Damocles abort scan. First, the CR3BP initial guess database is populated using the techniques described in previous sections. Using this database of information, Damocles calculates an approximate time-of-flight for its current node (this is a function of the launch day, launch time, mission phase, and EI day scan parameters) as well as the Abort Burn 1 (AB1) TIG scan parameter. Using these parameters, a least squares norm is used to determine the "closest" initial guess trajectory profile (as visualized by Figure 14(a)) to the current trajectory node. Initial guess data from the chosen trajectory must then be converted for use in Copernicus: Δv vectors are converted to alpha/beta angles for finite burns in a VUW maneuver frame, finite burn durations are calculated based on vehicle thrust and Isp values using the rocket equation, EI state vectors are converted to geographic coordinates in a body-fixed frame, and event epochs are converted from MET to absolute Ephemeris Times (ETs). Once the proper transformations are in place. this data is input into Copernicus as a set of OVs. Lastly, the convergence routine is called and the abort trajectory is optimized to minimize propellant consumption, an example of which is rendered in Figure 14 in the Earth-Moon rotating pulsating frame. Note that the general shape of the trajectory is maintained between the initial guess and the converged solution, and that forward-backward shooting is leveraged at each of the abort burn nodes to alleviate sensitivity in the process of transitioning to higher-fidelity. Ultimately, the initial guess provides an approximation of the maneuver cost and the time-of-flight for the given profile, while the higher-fidelity solution contains all system-level constraints imposed on the vehicle and ensures that an optimal abort trajectory is constructed for the given set of scan parameters.



Figure 13. Flowchart of Damocles Transcription Process.

CONCLUDING REMARKS

This investigation summarizes a process to generate families of abort trajectories in the Earth-Moon CR3BP for the upcoming Artemis missions. These families provide an understanding of the fundamental motion that is ultimately used to construct aborts in a higher-fidelity model. Using Periapsis Poincaré maps provides insight into the dominant motion through different regions of cislunar space such that seed trajectories are constructed to build these families of solutions. The multi-parameter continuation and optimization technique allows for the generation of locally Δv optimal solutions to be constructed in a dynamically sensitive solution space so that the abort families are classified based on their dynamical properties. The transcription process demonstrates how the initial guesses from various families can be used to construct and enforce system level constraints for a given mission. Lastly, optimization to a local propellant minimum solution in to a higher-fidelity Sun-Earth-Moon ephemeris model is achieved using the Copernicus and Damocles tools. This investigation seeks to demonstrate effective strategies to generate, classify and converge aborts in higher-fidelity models, allowing Artemis mission designers to make informed decisions pre-flight and in mission operations. A robust abort generation process ultimately makes Artemis missions more flexible and

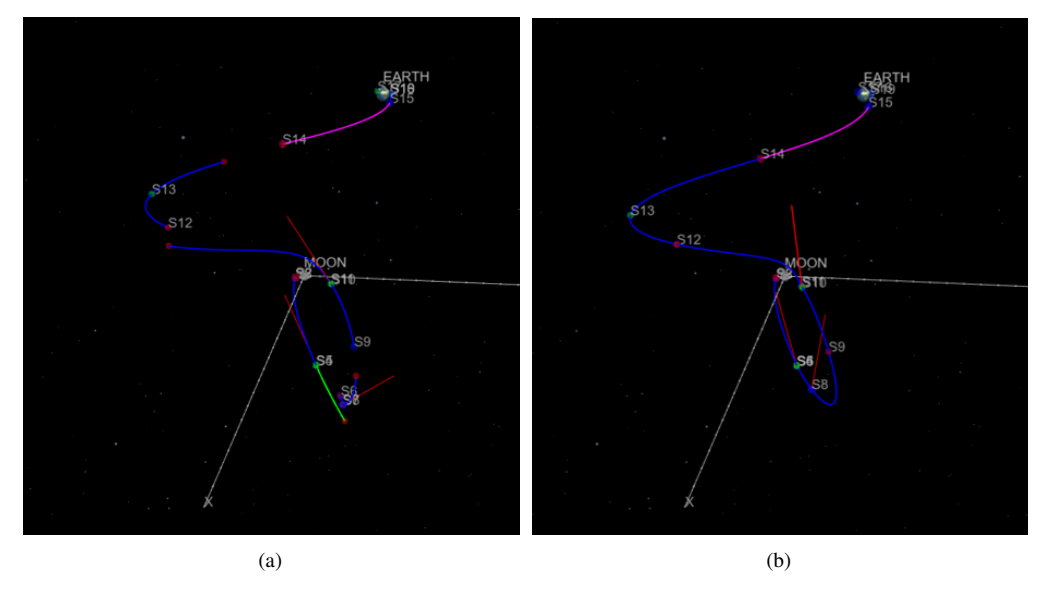


Figure 14. (a) Pre-converged three-burn initial guess from CR3BP transcribed into Copernicus. (b) Converged three-burn abort trajectory in Sun-Earth-Moon ephemeris model.

provides an understanding of the trajectory options in the event of an anomaly to return the crew to Earth safely.

ACKNOWLEDGEMENTS

The authors would like to thank Dale Williams and Rolfe Power for help in deriving the optimization constraint as well as Dave Lee, Colin Brown, and Robert Harpold for insightful discussions and guidance on the abort problem.

REFERENCES

- [1] K. Hambleton, T. Fairley, and L. Cheshier, "Splashdown! NASA's Orion Returns to Earth After Historic Moon Mission," *web*, Dec. 2022.
- [2] L. Mohon and C. Williams, "Artemis III: NASA's First Human Mission to the Lunar South Pole," web, January 2023. https://www.nasa.gov/missions/artemis/artemis-iii/.
- [3] C. T. Hyle, C. E. Foggatt, and B. D. Weber, "Apollo Experience Report Abort Planning," Tech Report NASA-TN-D-6847, NASA, Manned Spaceflight Center, June 1972.
- [4] C. E. Foggatt, "Two-Impulse Abort Maneuvers From A Lunar Mission," Technical Report NASA-TM-X-64395, National Aeronautics and Space Administration, Houston, TX, August 1966.
- [5] G. R. Babb, "Translunar Abort Techniques for Nonfree-Return Missions," Technical Report NASA-TM-X-1806, National Aeronautics and Space Administration, July 1969.
- [6] G. L. Condon, J. S. Senent, and E. G. Llama, "Abort Options for Human Lunar Missions between Earth Orbit and Lunar Vicinity," *AAS/AIAA Space Flight Mechanics Meeting*, Tampa, Florida, January 2006.
- [7] G. Condon, T. Dawn, R. Merriam, R. Sostaric, and C. H. Westhelle, "CEV Trajectory Design Considerations for Lunar Missions," AAS Guidance and Control Conference, Breckenridge, Colorado, February 2007.
- [8] R. J. Whitley, C. A. Ocampo, and J. Williams, "Performance of an Autonomous Multi-Maneuver Algorithm for Lunar Trans-Earth Injection," *Journal of Spacecraft and Rockets*, Vol. 49, February 2012.
- [9] J. Williams, E. C. Davis, D. E. Lee, G. L. Condon, and T. Dawn, "Global Performance of the Three Burn Trans-Earth Injection Maneuver Sequence over the Lunar Nodal Cycle," *AAS/AIAA Astrodynamics Specialist Conference*, August 2009.
- [10] S. Robinson and D. Geller, "A Simple Targeting Procedure for Lunar Trans-Earth Injection," AIAA Guidance, Navigation and Control Conference, Chicago, Illinois, August 2020.

- [11] T. Dong, Q. Luo, C. Han, and M. Xu, "Parameterized Design of Abort Trajectories with a Lunar Flyby for a Crewed Mission," *Advances in Space Research*, Vol. 71, pp. 2550–2565.
- [12] R. E. Harpold, C. Brown, B. J. Killeen, R. A. Eckman, T. F. Dawn, B. Adebonojo, and J. Williams, "Arteims I Off-Nominal Trajectory Design and Optimization," *AAS/AIAA Astrodynamics Specialist Conference*, Big Sky, Montana, August 2023.
- [13] A. Batcha, J. Williams, T. F. Dawn, J. P. Gutkowski, M. Widner, S. L. Smallwood, B. J. Killeen, E. C. Williams, and R. E. Harpold, "Artemis 1 Trajectory Design and Optimization," AAS/AIAA Astrodynamics Specialist Conference, Virtual, Aug. 2020.
- [14] V. Szebehely, *The Theory of Orbits: The Restricted Problem of Three Bodies*. New York, New York: Academic Press, Inc, 1967.
- [15] C. H. Acton, Ancillary Data Services of NASA's Navigation and Ancillary Information Facility, Jan. 1996. https://naif.jpl.nasa.gov/naif/.
- [16] L. Kaufman, "A Variable Projection Method for Solving Separable Nonlinear Least Squares Problems," BIT Numerical Mathematics, Vol. 15, March 1975, pp. 49–57.
- [17] J. Goodman, "Newton's Method for Constraint Optimization," *Mathematical Programming*, Vol. 33, November 1985, pp. 162–171, https://doi.org/10.1007/BF01582243.
- [18] M. E. Henderson, "Multiple Parameter Continuation: Computing Implicitly Defined *k*-Manifolds," *International Journal of Bifurfactions and Chaos*, Vol. 12, June 2001, pp. 451–476.
- [19] B. McCarthy, S. Scheuerle, E. Zimovan-Spreen, D. Williams, D. Davis, and K. Howell, "Rephasing and Loitering Strategies in the Gateway Near Rectilinear Halo Orbit," AAS/AIAA Astrodynamics Specialist Conference, Big Sky, Montana, August 2023.
- [20] D. C. Davis, S. M. Phillips, and B. P. McCarthy, "Multi-Body Mission Design Using the Deep Space Trajectory Explorer," *26th AAS/AIAA Spaceflight Mechanics Meeting*, Napa, California, Feb. 2016.
- [21] D. C. Davis, S. M. Phillips, and B. P. McCarthy, "Periapsis Poincaré Maps for Preliminary Trajectory Design in Planet-Moon Systems," AAS/AIAA Astrodynamics Specialist Conference, Vail, Colorado, Aug. 2015.
- [22] D. C. Davis, S. M. Phillips, and B. P. McCarthy, "Trajectory Design for Saturnian Ocean Worlds Orbiters Using Multidimensional Poincaré Maps," *Acta Astronautica*, Vol. 143, Feb. 2018, pp. 16–28.
- [23] B. McCarthy, J. Petersen, and D. C. Davis, "Ballistic Lunar Transfer Design Using the Deep Space Trajectory Explorer," 33rd AAS/AAIA Spaceflight Mechanics Meeting, Austin, Texas, June 2023.
- [24] D. Henry and D. J. Scheeres, "Fully numerical computation of heteroclinic connection families in the spatial three-body problem," *Communications in Nonlinear Science and Numerical Simulation*, Vol. 130, March 2024, https://doi.org/10.1016/j.cnsns.2023.107780.
- [25] B. McCarthy and K. Howell, "Four-body cislunar quasi-periodic orbits and their application to ballistic lunar transfer design," *Advances in Space Research*, Vol. 71, Jan. 2023.
- [26] S. Scheuerle and K. Howell, "Tidal Attributes of Low-energy Transfers in the Earth-Moon-Sun System," *AAS/AIAA Astrodynamics Specialist Conference*, Charlotte, North Carolina, Aug. 2022.
- [27] M. E. Paskowitz and D. J. Scheeres, "Robust Capture and Transfer Trajectories for Planetary Satellite Orbiters," *Journal of Guidance, Control, and Dynamics*, Vol. 29, Mar. 2006.
- [28] M. E. Paskowitz and D. J. Scheeres, "Design of Science Orbits About Planetary Satellites: Application to Europa," *Journal of Guidance, Control, and Dynamics*, Vol. 29, No. 5, 2006, pp. 1147–1158.
- [29] M. Ceriotti and C. R. McInnes, "Design of Ballistic Three-Body Trajectories for Continuous Polar Earth Observation in the Earth-Moon System," *Acta Astronautica*, Vol. 102, October 2014, pp. 178–189.
- [30] R. W. Farquhar and D. W. Dunham, "A New Trajectory Concept for Exploring Earth's Geomagnetic Tail," *Journal of Guidance and Control*, Vol. 4, March 1981.
- [31] C. Uphoff, "The Art and Science of Lunar Gravity Assist," *AAS/NASA International Symposium*, Greenbelt, Maryland, April 1989.
- [32] J. Rhea, "Exploration Mission Entry Interface Target Line," techreport, NASA Johnson Space Center.
- [33] J. Williams, A. Kamath, R. Eckman, G. Condon, R. Mathur, and D. Davis, "Copernicus 5.0: Latest Advances in JSC's Spacecraft Trajectory Optimization and Design System," *AAS/AIAA Astrodynamics Specialist Conference*, Portland, Maine, August 2019.
- [34] C. A. Ocampo, "An Architecture for a Generalized Trajectory Design and Optimization System," *International Conference on Libration Points and Missions*, Aiguablava, Spain, June 2002.
- [35] Q. Moore, B. Killeen, and J. Williams, "A New Architecture for Parallelization of Complex Spacecraft Trajectory Optimization Scans," AAS/AIAA Astrodynamics Specialist Conference, Big Sky, Montana, August 2023.
- [36] D. Owen, M. Bolliger, G. Savidge, A. Heritier, and B. McCarthy, "A Framework for Moving Artemis Abort Trajectories from the CR3BP to a High-Fidelity Ephemeris Model," AAS/AIAA Astrodynamics Specialist Conference, Broomfield, Colorado, August 2024.